



University of  
Zurich<sup>UZH</sup>

Zurich Open Repository and  
Archive

University of Zurich  
Main Library  
Strickhofstrasse 39  
CH-8057 Zurich  
[www.zora.uzh.ch](http://www.zora.uzh.ch)

---

Year: 2018

---

## Evolution of soil erosion rates in alpine soils of the Central Rocky Mountains using fallout Pu and <sup>13</sup>C

Portes, Raquel ; Dahms, Dennis ; Brandová, Dagmar ; Raab, Gerald ; Christl, Marcus ; Kühn, Peter ; Ketterer, Michael ; Egli, Markus

**Abstract:** Data from soil chronosequences have been widely used to quantify soil formation and weathering rates, but are less used to determine erosion rates and the stabilisation of moraines over time. We hypothesise that soil erosion rates on moraine hillslopes decrease over time as soils evolve and slopes stabilise. We selected a sequence of moraines in the Wind River Range (Central Rocky Mountains) to study these processes over time. Moraine ages were based on <sup>10</sup>Be surface exposure dating of moraine boulders. Quantitative soil erosion and accumulation rates along slopes with similar exposures, lengths and gradients were determined from profile patterns of <sup>239</sup>+<sup>240</sup>Pu radionuclides. We used stable carbon isotopes (<sup>13</sup>C) in relation with the total soil organic carbon (SOC) content for qualitative information about soil erosion. The <sup>10</sup>Be boulder exposure ages revealed that the moraines were deposited during the Younger Dryas and the pre Bølling–Allerød episodes of the late Pleistocene. The morphology of the soils suggests a complex history of development and shows that both erosion and aeolian deposition have affected the soils. The <sup>239</sup>+<sup>240</sup>Pu measurements revealed that erosion rates strongly decrease with time as soils develop. A weakly developed soil (Cambisol) is found on the youngest moraine (11.8 ka) that exhibits an erosion rate, depending on the calculation procedure, in the range of 260 to 520 t km<sup>-2</sup> a<sup>-1</sup>. With time the erosion rate rapidly decreases to almost zero, presumably as a full vegetation cover develops. Bioturbation and/or dust influx is increasingly obvious with increasing age of the soils, as evidenced by the comparison of <sup>13</sup>C and SOC. The mass balance of the oldest soil (15.8 ka) indicates that the slopes have reached a geomorphological stability with little or no net erosion. Aeolian influx appears to be the primary factor to account for mass changes in the oldest soil.

DOI: <https://doi.org/10.1016/j.epsl.2018.06.002>

Posted at the Zurich Open Repository and Archive, University of Zurich

ZORA URL: <https://doi.org/10.5167/uzh-161310>

Journal Article

Accepted Version



The following work is licensed under a Creative Commons: Attribution-NonCommercial-NoDerivatives 4.0 International (CC BY-NC-ND 4.0) License.

Originally published at:

Portes, Raquel; Dahms, Dennis; Brandová, Dagmar; Raab, Gerald; Christl, Marcus; Kühn, Peter; Ketterer, Michael; Egli, Markus (2018). Evolution of soil erosion rates in alpine soils of the Central Rocky

Mountains using fallout Pu and  $^{13}\text{C}$ . Earth and planetary science letters, 496:257-269.  
DOI: <https://doi.org/10.1016/j.epsl.2018.06.002>

# 1 Evolution of soil erosion rates in alpine soils of the Central Rocky Mountains using 2 fallout Pu and $\delta^{13}\text{C}$

3  
4 Raquel de Castro Portes<sup>1\*</sup>, Dennis Dahms<sup>2</sup>, Dagmar Brandová<sup>1</sup>, Gerald Raab<sup>1</sup>, Marcus Christl<sup>3</sup>, Peter  
5 Kühn<sup>4</sup>, Michael Ketterer<sup>5</sup>, Markus Egli<sup>1</sup>

6  
7 <sup>1</sup>Department of Geography, University of Zurich, Winterthurerstrasse 190, CH-8057 Zurich, Switzerland

8 <sup>2</sup>Department of Geography, University of Northern Iowa, Cedar Falls, IA 50614-0406, USA

9 <sup>3</sup>Laboratory of Ion Beam Physics, ETH Zurich, 8093 Zurich, Switzerland

10 <sup>4</sup>Research Area Geography, Soil Science and Geomorphology, Department of Geosciences, University of  
11 Tübingen, Rümelinstrasse, 19-23, 72070 Tübingen, Germany

12 <sup>5</sup>Chemistry Department, Metropolitan State University of Denver, Campus Box 52, Denver, CO 80217-3362,  
13 USA

## 14 15 **Abstract**

16 Data from soil chronosequences have been widely used to quantify soil formation and weathering rates, but  
17 are less used to determine erosion rates and the stabilisation of moraines over time. We hypothesise that  
18 soil erosion rates on moraine hillslopes decrease over time as soils evolve and slopes stabilise. We selected  
19 a sequence of moraines in the Wind River Range (WRR; Central Rocky Mountains) to study these  
20 processes over time. Moraine ages were based on <sup>10</sup>Be surface exposure dating of moraine boulders.  
21 Quantitative soil erosion and accumulation rates along slopes with similar exposures, lengths and gradients  
22 were determined from profile patterns of <sup>239+240</sup>Pu radionuclides. We used stable carbon isotopes ( $\delta^{13}\text{C}$ ) in  
23 relation with the total soil organic carbon (SOC) content for qualitative information about soil erosion. The  
24 <sup>10</sup>Be boulder exposure ages revealed that the moraines were deposited during the Younger Dryas and the  
25 pre Bølling–Allerød episodes of the late Pleistocene. The morphology of the soils suggests a complex history  
26 of development and shows that both erosion and aeolian deposition have affected the soils. The <sup>239+240</sup>Pu  
27 measurements revealed that erosion rates strongly decrease with time as soils develop. A weakly developed  
28 soil (Cambisol) is found on the youngest moraine (11.8 ka) that exhibits an erosion rate, depending on the  
29 calculation procedure, in the range of 260 to 520 t km<sup>-2</sup> a<sup>-1</sup>. With time the erosion rate rapidly decreases to  
30 almost zero, presumably as a full vegetation cover develops. Bioturbation and/or dust influx is increasingly  
31 obvious with increasing age of the soils, as evidenced by the comparison of  $\delta^{13}\text{C}$  and SOC. The mass

32 balance of the oldest soil (15.8 ka) indicates that the slopes have reached a geomorphic stability with little or  
33 no net erosion. Aeolian influx appears to be the primary factor to account for mass changes in the oldest soil.

34

35 **Keywords:** Slope stability, Pu isotopes, carbon isotopes, soil chronosequence, Late Pleistocene, Wind River  
36 Range

37

38 \*Correspondent author: +41 44 63 55179

39 E-mail address: raquel.decastroportes@geo.uzh.ch (R. C. Portes)

40

41

## 42 **1. Introduction**

43 To date, most studies evaluating rates of soil erosion have focused on the impact of soil tillage on  
44 agricultural lands (Quine and Walling, 1991) and on the comparison between cultivated and uncultivated  
45 soils (He and Walling, 1997; Lal et al., 2013; Zhang et al., 1990), while few have focused on natural  
46 environments, such as forested slopes (Meusburger et al., 2013) or high alpine areas (Zollinger et al., 2015).

47 We know of no studies, to date, that concern how rates of erosion (or accumulation) evolve as a function of  
48 time and soil development.

49 Besides slope gradient and soil cover, soil erodibility is strongly linked to soil characteristics such as particle  
50 size distribution, stoniness, structure, permeability, water content and organic matter content (Wischmeier  
51 and Smith, 1960; Lal and Elliot, 1994). Numerous studies demonstrate that these soil characteristics change  
52 over time as soils evolve (Dahms et al., 2012). Soil chronosequences are a powerful tool widely used on  
53 moraine sequences to examine soil development over time. Because they enable us to estimate rates of soil  
54 formation (Bockheim, 1980; Huggett, 1998; Dahms et al., 2012.) this approach also can be useful to evaluate  
55 the evolution of soil erosion rates over time. Soils of different ages may therefore give valuable insight into  
56 the temporal evolution of soil erosion. When suitable sites are available, radionuclides have been shown to  
57 be good tracers for estimates of soil erosion.

58 Fallout radionuclides (FRNs) (e.g.  $^{137}\text{Cs}$  and  $^{139+140}\text{Pu}$ ) have been widely used to trace mid-term (decadal)  
59 soil erosion (or accumulation) rates in natural and agricultural areas worldwide (Alewell et al., 2014; He and  
60 Walling, 1997). FRNs were mainly emitted to the upper atmosphere by above-ground nuclear weapons  
61 testing during the 1950-1960's and/or by nuclear reactor accidents (e.g. Chernobyl 1986). When deposited  
62 on the soil surface, they strongly bond to solid phases due to their high ionic potential, which makes them

63 insoluble. Therefore, their removal from soil can be associated with soil erosion processes more directly than  
64 chemical (leaching), translocation or biological processes (Ketterer et al., 2011). FRNs inventories provide  
65 information of soil mass movement per unit area only over the past 50 – 60 years (Alewell et al., 2014; Lal  
66 and Elliot, 1994). The rates are estimated by comparing tracer inventory at various soil depths to a nearby  
67 non-eroding reference site. The reference site is assumed to have negligible soil erosion or deposition, thus  
68 each site represents the total tracer inventory (He and Walling, 1996). The tracer inventory in non-eroding  
69 sites is lost by radioactive decay, while erosional sites lose tracer by both decay and erosion (Lal et al.,  
70 2013). The correlation of stable carbon isotopes signatures (i.e.  $\delta^{13}\text{C}$ ) and soil organic carbon content can  
71 qualitatively indicate long-term disturbances in aerated soils, where high correlations reflects the enrichment  
72 of  $^{13}\text{C}$  in depth as soil organic carbon decomposes in non-eroded soils (Alewell and Schaub, 2009;  
73 Meusburger et al., 2013; Zollinger et al., 2015). Due to isotopic fractionation during plant decomposition,  
74 residues are increasingly enriched in the heavier carbon isotope ( $^{13}\text{C}$ ) as the lighter  $^{12}\text{C}$  will preferentially be  
75 involved in biochemical reactions (Alewell and Schaub, 2009). In undisturbed soils, therefore, increasing  
76  $\delta^{13}\text{C}$  values and decreasing total org. C contents with depth would be typical and should correlate with the  
77 pattern of erosion rates determined by the Pu-isotopes.

78 In this study, we test the hypothesis that soil erosion rates on moraine hillslopes decrease over time as soils  
79 evolve. To test this hypothesis, we chose a location in the Wind River Range (WRR; Central Rocky  
80 Mountains) with a previously-described and mapped sequence of moraines and slopes related to post-LGM  
81 (Last Glacial Maximum; post-Pinedale) glacial activity (Dahms et al., 2010). Hence, our objective is to  
82 quantitatively assess soil erosion or accumulation rates using a chronosequence approach combined with  
83 fallout radionuclides ( $^{239+240}\text{Pu}$ ). In addition, we expected that  $\delta^{13}\text{C}$  and organic C in the soils correlate most  
84 strongly with increasing age of the soils and decreasing rates of erosion. Erosion rates were – with purpose  
85 – not investigated using cosmogenic nuclides (such as  $^{10}\text{Be}$  and others). These isotopes only give an  
86 average value over the entire period of pedogenesis. To better trace the evolution of soil erosion, moraine  
87 slopes having a different age should be investigated by using isotopes that give a more instantaneous signal.  
88 FRNs are ideal tracers for this purpose and reflect the actual state (i.e last few decades). Using this  
89 approach, we should be able to quantify soil erosion over time on moraine slopes in an alpine area and to  
90 approximate the age(s) during which these moraines are stabilised and erosional losses minimised.

91

## 92 **2. Study area**

93 The Wind River Range (WRR) is located in the central Rocky Mountains of west-central Wyoming, USA (Fig.

94 1a). The range trends Northwest-Southeast with a length of approximately 225 km and a width of 48 km (Fig.  
95 1b; Dahms, 2002; Keefer, 1970). The lithology of the range is mainly composed of early Precambrian  
96 granitoid batholith (Keefer, 1970). Sedimentary rocks with different ages and compositions surround the  
97 batholith's range: Eocene sandstones and shales bound the west flank while Paleozoic and Mesozoic  
98 limestones, siltstones and sandstones form hogback ridges along the eastern flank of the range (Keefer,  
99 1970). The WRR belongs entirely to the Greater Yellowstone Ecosystem and its major part to the Bridger-  
100 Teton and Shoshone national forests and wilderness areas. Vegetation is characterised by alpine tundra  
101 above ~3200 meters and conifer forest below (Dahms et al., 2010). In the Cirque of the Towers (Fig. 1 a,b;  
102 located in the southern WRR), mean annual precipitation varies around 1100 mm/yr and mean annual  
103 temperature is about -3.7 °C (Dahms, 2002).

104 First investigations of allostratigraphic units in the WRR (alpine to high alpine areas; from the northern to the  
105 southern parts of the WRR) and soils were reported by Dahms et al. (2010). In general, the soils are rather  
106 shallow but enable a distinction of younger from older moraine deposits. The soils vary from Lithosols  
107 (youngest soils) to Luvisol or Cambisols with transition to Podzols (oldest soils). Two types of B horizons  
108 were recognised; those based mainly on colour are Bw horizons, whereas those based on both colour and  
109 an increase in clay content are Bt horizons (Dahms et al., 2010). Typically, many soils exhibit a thin loess  
110 mantle that has been deposited since the end of the last glaciation. Several studies have demonstrated that  
111 much of the silt and clay in soils developed on alpine moraines in the WRR has an atmospheric origin, which  
112 is evidenced by aeolian signals in the particle size distribution, heavy mineral fractions and geochemical  
113 signatures (Applegarth and Dahms, 2004; Dahms and Rawlins, 1996).

114 Due to the relatively dry environmental conditions, dust input is not only related to glacial periods; there also  
115 is evidence for modern-day aeolian inputs to soils of the WRR (Applegarth and Dahms, 2004; Dahms and  
116 Rawlins, 1996). Dust particles are those that have been entrained by the wind and transported without  
117 contact with the ground surface. This distinguishes dust particles (mainly coarse-to-medium silt) from larger  
118 grains, such as sand, that can also be transported by the wind. Sand-sized particles, when transported by  
119 the wind, do so largely by saltation, a bouncing type of particle motion with periodic contact with the ground  
120 surface, or by surface creep, where there is constant contact with the ground surface during horizontal  
121 transport (Muhs, 2013). Loess is recognised in the field by its silt loam texture which contrasts markedly with  
122 the underlying gritty sandy loam or loamy sand matrix (Shroba and Birkeland, 1983). Horizons with some  
123 loess can be loamy when silt loam loess is mixed with coarser materials.

124

### 125 **3. Materials and methods**

### 126 3.1. Experimental set-up and soil sampling

127 The Cirque of the Towers (Fig. 1a, b) was chosen as study site because of its well-mapped sequence of  
128 moraines related to post-LGM (post-Pinedale) glacial activity (Dahms et al., 2010). Based on Dahms et al.'s  
129 (2010) map of this cirque, we selected a sequence of three moraines with different, relative age estimates.  
130 To better constrain our age constraints, the moraines were dated using surface exposure dating ( $^{10}\text{Be}$ ) of  
131 moraine boulders. The moraines were selected based on published maps of the WRR showing the late  
132 Quaternary glacial and periglacial deposits (Dahms et al., 2010). These authors correlated the  
133 allostratigraphic units and assigned them to the Holocene (e.g. Alice Lake alloformation) and Pleistocene  
134 (e.g. Temple Lake alloformation). No numeric ages were presented. We sampled moraine boulders for  
135 surface exposure dating ( $^{10}\text{Be}$ ) according to the sampling guidelines of Gosse and Phillips (2001). We chose  
136 large, flat-topped boulders to avoid edge effects protruding more than 2m from the surrounding sediments  
137 (Masarik and Wieler, 2003). The position (latitude/longitude and altitude) of the sample sites was recorded  
138 with GPS and verified with topographic maps. The geometry of each boulder and the effect of topographic  
139 shielding by surrounding mountains were assessed. Because cosmic rays are distinctly attenuated within the  
140 rock material, production of cosmogenic isotopes is highest at the surface; thus, we sampled the uppermost  
141 1-3 centimetres of the rock surface and documented the sample thickness.

142 On each of the three moraines (Alice Lake, Temple Lake and Lonesome Lake), we proceeded as follows:

143 i) We sampled one soil profile at the crest (Fig. 1c; Table 1). Soil pits were excavated to the C horizon where  
144 possible. Soil descriptions were carried out according to FAO guidelines (FAO, 2006) and the soils classified  
145 according to IUSS Working Group WRB (2015). Vegetation cover was estimated at each site on the basis of  
146 visual examination in the field (in % cover; ocular estimation of the cover; done as 'canopy' cover; Whittaker,  
147 1962). Root abundance and size in the profiles were assessed following FAO (2006).

148 ii) For the determination of soil erosion and accumulation rates using  $^{239+240}\text{Pu}$  and  $\delta^{13}\text{C}$ , we sampled on  
149 each moraine:

150 - 'Reference' profiles (0 – 20 cm; using a soil corer) at undisturbed flat locations on each moraine  
151 where erosion and accumulation processes could reasonably be assumed to be negligible for the  
152 last 50 to 60 years (that corresponds to the time range covered by Pu-isotopes).

153 - 'Erosion sites' (0 – 20 cm; using a soil corer) that were located on the backslope of the moraines  
154 with north to northeast aspects, slope inclinations of 25% and lengths of 15 – 21 m (Table 1).  
155 Erosion or accumulation rates were always calculated in comparison to the corresponding reference  
156 site.

157 - We took four replicate profiles at each of the reference and erosion sites. Soil samples for  $^{239+240}\text{Pu}$ ,  
158  $\delta^{13}\text{C}$  and org. C analyses were taken from the soil corer at 5 cm increments from 0 – 20 cm depths.  
159 The soil cores were also used to determine bulk densities.

160

### 161 3.2. Soil analyses

162 Samples were oven-dried at 70°C and sieved (<2 mm) prior to analysis. Prior to grain size analysis, 60 g of  
163 fine earth were dispersed in a 3%  $\text{H}_2\text{O}_2$  solution to digest soil organic matter. The grain size distribution was  
164 determined by combination of wet-sieving of the coarser particles (2000 - 32  $\mu\text{m}$ ) and X-ray granulometry  
165 (SediGraph 5100) measurements for the finer particles (32 - 1  $\mu\text{m}$ ). Soil pH was determined using a  
166 soil:solution (0.01M  $\text{CaCl}_2$ ) ratio of 1:2.5.

167 The  $\delta^{13}\text{C}$  signature tends to become less negative with soil depth due to the relative increase in the heavier  
168  $^{13}\text{C}$  (Alewell and Schaub, 2009). We expected that the change in  $\delta^{13}\text{C}$  content with soil depth would parallel  
169 the decrease in carbon content. Soil erosion processes have been shown to weaken this correlation (Alewell  
170 and Schaub 2009; Zollinger et al., 2015). The  $\delta^{13}\text{C}$  isotopic ratios were measured using a Picarro analyser  
171 (G2131-i Picarro) for isotopic  $\text{CO}_2$  (Combustion Module-Cavity Ring Down Spectroscopy (CM-CRDS),  
172 Sunnyvale, California, USA). Instrumental measurement uncertainty is 0.1%. Soil powder (milled fine earth)  
173 was weighed into tin capsules and combusted at 950 °C. The released  $\text{CO}_2$  was measured using a CRDS  
174 analyser (Picarro, G2131 type). We used an internal standard (30B00GW9 Chernozem 2013) for every 6  
175 samples in order to correct for potential drift in the  $\delta^{13}\text{C}$  and C content values.

176 We used the rock fragments and several fractions of the fine earth as diagnostic criteria for the identification  
177 of any lithologic discontinuities in the profile (Schaetzl, 1998; FAO, 2006).

178

### 179 3.3. Sample preparation and measurement for $^{10}\text{Be}$ surface exposure dating

180 Cosmogenic nuclides can be used for both surface age determination and calculation of erosion or  
181 denudation rates (Balco et al., 2008). In our case, we used  $^{10}\text{Be}$  for deriving age constraints of the  
182 investigated moraines. We obtained numeric age-estimates for the moraines from  $^{10}\text{Be}$  surface exposure  
183 dating of two large granitic boulders (> 2m in height) on each moraine. The rock samples were pre-treated  
184 following the procedures according to Kohl and Nishiizumi (1992). Samples were crushed and sieved and  
185 the quartz isolated by treating the 0.25 mm – 0.6 mm fraction with *aqua regia* to destroy organic  
186 contaminations and any calcareous components. After a 1h-treatment with 0.4% HF, we used a floatation  
187 system to physically separate feldspar and mica components from quartz. Remaining non-quartz remnants



188 were removed by repeated leaching by 4%HF. Once pure quartz was obtained, we added a  $^9\text{Be}$ -carrier  
189 solution and dissolved the samples in 40%HF. Be was isolated using anion and cation exchange columns  
190 followed by selective pH precipitation techniques (Von Blanckenburg et al., 1996). The Be hydroxides then  
191 were precipitated, dried, and calcinated to BeO at 850°C.  $^{10}\text{Be}/^9\text{Be}$  ratios were measured at the ETH  
192 Laboratory of Ion Beam Physics' Accelerator Mass Spectrometry (AMS) facility using the  $^{10}\text{Be}$  standard  
193 S2007N with a nominal value of  $^{10}\text{Be}/^9\text{Be} = 28.1 \times 10^{-12}$  (Christl et al., 2013). S2007N has been calibrated to  
194 the  $^{10}\text{Be}$  standard ICN 01-5-1 of Nishiizumi (2007) and has a nominal  $^{10}\text{Be}/^9\text{Be}$  value of  $2.709 \times 10^{-11}$ . The  $1\sigma$   
195 error of S2007N is 2.7% (Christl et al., 2013). Measured  $^{10}\text{Be}/^9\text{Be}$  ratios were corrected for  $^{10}\text{Be}$  contributed  
196 by the Be-carrier (blank value: 0.003E-12).  $^{10}\text{Be}$  concentrations and according one sigma uncertainties are  
197 reported in Table 2.  $^{10}\text{Be}$  exposure ages were calculated using CRONUS-Earth  
198 (<http://hess.ess.washington.edu/math/>) version 2.3 with a  $^{10}\text{Be}$  half-life of  $1.387 \pm 0.012$  Ma (Chmeleff et al.,  
199 2010). The production rate was corrected for latitude and altitude using the scaling scheme of Stone (Stone,  
200 2000) and corrected for sample thickness assuming an exponential depth profile with an effective radiation  
201 attenuation length of  $160 \text{ g cm}^{-2}$  (Gosse and Phillips, 2001) and a rock density of  $2.7 \text{ g cm}^{-3}$ . Effects of  
202 variations of the geomagnetic field on the  $^{10}\text{Be}$  age are said to be negligible (Pigati and Lifton, 2004).

203

#### 204 3.4. Sample preparation and measurement for $^{239+240}\text{Pu}$ activities

205 Sample preparation was done according to Ketterer et al. (2004). The samples obtained from the soil cores  
206 (erosional and reference sites) were analysed for  $^{239+240}\text{Pu}$ . Five grams of the milled fine earth ( $\approx 60\mu\text{m}$ ) was  
207 dry-ashed for 20 hours at 600 °C to remove organic matter. A spike of ca. 30 picograms (0.0044 Bq) of  $^{242}\text{Pu}$   
208 tracer solution (NIST 4334) was added to the sample vials. The samples were then leached using 10 mL of  
209 16 M  $\text{HNO}_3$  in a heating oven at 75 °C for 20 hours. After acid leaching, the samples were filtered into a 50  
210 mL centrifuge tube and adjusted to a concentration of 8 M  $\text{HNO}_3$ . Pu species were adjusted to a  $\text{Pu}^{4+}$   
211 oxidation state using an acidified  $\text{FeSO}_4 \cdot 7\text{H}_2\text{O}$  solution (2 mg/mL of leached solution) and  $\text{NaNO}_2$  solution  
212 (20 mg/mL of solution). The  $\text{Fe}^{2+}$  solution was added first and subsequently the sodium nitrite solution.  
213 Thereafter, the samples were heated at 75 °C for 2 hours. After the oxidation process, TEVA resin (Triskem-  
214 international 100-150  $\mu\text{m}$ ; 2 mg of TEVA per mL of leached solution) was added to the centrifuge tubes and  
215 shaken using a horizontal shaker for 2 hours so that the TEVA uptakes the tetravalent Pu. Thereafter the  
216 resin was collected using a pipet tip containing glass wool plug. The pipet tips were rinsed to remove  
217 tetravalent actinides (i.e. U and Th) using acid solutions in the following order: 5 x 2 M  $\text{HNO}_3$ ; 3 x 8 M  $\text{HCl}$ ; 2  
218 x 2 M  $\text{HNO}_3$  (rinse volume: 1ml per 30 mg of TEVA). Pu was eluted into Eppendorf tubes using 0.4 ml 0.05 M

219 ammonium oxalate and diluted with water to a 1.2 ml final volume. Each batch contained 37 samples and 13  
220 controls: 3 pre-bomb soils as a 'negative control', 2 Standard Reference Material 4350b (river sediment for  
221 radioactivity measurements from NIST), 3 blanks and 5 duplicates of soil samples.

222 The measurements of Pu isotopes were carried out using an Agilent 8800 Triple Quadrupole ICP-MS. The  
223 ICP-MS instrument was equipped with a high-efficiency desolvating sample introduction system (APEX HF,  
224 ESI Scientific, Omaha, NE, USA). A detection limit of  $< 0.1$  Bq/kg  $^{239+240}\text{Pu}$  was obtained for samples of  
225 nominal 1 gram of dry-ashed material; for  $^{239+240}\text{Pu}$  activities  $> 1$  Bq/kg, the measurement error was 1 to 3 %.

226  
227 3.5. Conversion of  $^{239+240}\text{Pu}$  activities into soil erosion and accumulation rates

228 The inventories (Bq/m<sup>2</sup>) of  $^{239+240}\text{Pu}$  were calculated based on the following equation:

$$229 \quad A(s) = \frac{1}{S} \sum_i M_{Ti} C_i \quad (1)$$

230 Where  $C_i$  is the activity of the  $i$ th sub-sample depth increment (Bq/kg);  $M_{Ti}$  is the total mass of the  $i$ th sample  
231 depth increment (kg) and  $S$  is the area of the horizontal core cross (m<sup>2</sup>). Soil erosion or accumulation rates  
232 were calculated by comparing the isotope inventory for an eroding site with the corresponding inventory of  
233 the reference site where neither erosion nor soil accumulation are assumed.

234 Then, two different models were used to convert  $^{239+240}\text{Pu}$  inventories into soil erosion rates.

235 1) The profile distribution model (PDM) according to Walling and Quine (1990) and Zhang et al. (1990):

$$236 \quad A'(x) = A_{\text{ref}}(1 - e^{x/h_0}) \quad (2)$$

237 Where  $A'(x)$  is the amount of isotope inventory above depth  $x$  (Bq/m<sup>2</sup>),  $x$  is the depth from soil surface  
238 expressed as mass between top and actual depth (kg/m<sup>2</sup>),  $A_{\text{ref}}$  is the reference inventory as mean of all  
239 reference sites (Bq/m<sup>2</sup>) and  $h_0$  is the profile shape factor (kg/m<sup>2</sup>) that is a coefficient describing the rate of  
240 exponential decrease in inventory with depth for soil profiles in uncultivated sites.

241 The erosion rate  $Y$  was calculated according to Walling and He (1999) and Zhang et al., (1990):

$$242 \quad Y = \frac{10}{t-t_0} \times \ln\left(1 - \frac{X}{100}\right) \times h_0 \quad (3)$$

243 Where  $Y$  is erosion rate (t/ha/year),  $t$  is the year of sampling (i.e. 2016),  $t_0$  is a reference year (i.e. 1963) for  
244 thermonuclear weapon testing commonly used in for  $^{239+240}\text{Pu}$ ,  $X$  is % reduction of total inventory ( $A_u$  [Bq/m<sup>2</sup>])  
245 in relation to the local reference value ( $(A_{\text{ref}} - A_u)/A_{\text{ref}} \times 100$ ).

246 2) The inventory method (IM) according to Lal et al. (2013):

$$247 \quad L = -\frac{1}{\alpha P} \ln\left(1 - \frac{I_{\text{loss}}}{I_{\text{ref}}}\right) \quad (4)$$

248 Where  $L$  is loss of soil,  $I_{\text{loss}}$  is  $I_{\text{ref}} - I$ ,  $I_{\text{ref}}$  is the local reference inventory as mean of all reference sites (Bq/m<sup>2</sup>)  
249 and  $P$  is particle size correction factor, where  $P > 1$ . Corrections were done using a  $P$  factor of 1 and 1.2

250 according to Walling and He (1999) and 1.5 according to Lal et al., (2013). These factors take into account  
251 that erosion processes act in a selective way, removing or depositing fine particles and because of Pu is  
252 preferentially adsorbed in such fine particles (He and Walling, 1996), we used these correction factors to  
253 avoid overestimation of the soil erosion rates. The coefficient  $\alpha$  was obtained from a least squared  
254 exponential fit of the  $^{239+240}\text{Pu}$  depth profile (Alewell et al., 2014).

255

## 256 **4. Results**

### 257 4.1. $^{10}\text{Be}$ Surface exposure ages

258  $^{10}\text{Be}$  measurements of the moraine boulders (Table 2) show that the Alice Lake (P1 in Fig. 1c, Table 1)  
259 moraine is the youngest, with ages of 11.3 and 12.4 ka (considering the internal errors and error  
260 propagation, this gives an average age of  $11.8 \pm 0.3$  ka). Ages of the boulders on the Temple Lake (P2 in  
261 Fig. 1c, Table 1) and Lonesome Lake (P3 in Fig. 1c, Table 1) moraines are quite similar. Exposure ages of  
262 the Temple Lake moraine boulders are 15.2 and 15.9 ka (average age =  $15.5 \pm 0.3$  ka) and the ages of  
263 boulders on the Lonesome Lake moraine are 15.3 and 16.3 ka (average age =  $15.8 \pm 0.3$  ka).

264

### 265 4.2. Soil morphological and physical characteristics

266 Soils on moraines in the Cirque of the Towers have developed on granitic till. All soils are acidic with a pH in  
267 the range of 4.3 to 5.0 in the topsoil, have a high organic carbon content in their uppermost horizons and  
268 show a trend of increasing bulk density with depth (Table 3). Bulk density values with  $0.8$  to  $1.0 \text{ g/cm}^3$  are  
269 rather low in the upper horizon of the soils due to the low soil skeleton proportion. In addition, organic matter  
270 is present to a relatively great depth which contributes to the low bulk densities. All investigated soils exhibit  
271 two lithologic discontinuities that was evidenced by a textural change and an increase in coarse fragments  
272 with depth (Table 4).

273 Profiles P1 (Alice Lake moraine) and P2 (Temple Lake moraine) are classified as Cambisols (Reference Soil  
274 Group – RSG). In profile P1, the content of coarse fragments ( $> 2$  mm) increases with depth, from about 5%  
275 in the A1 horizon to about 38% in the 3Cox/Bw horizon. The A1 and 2A2 horizons have sandy loam textures  
276 and the 2Bw horizon is loam and the 3Cox/Bw horizon is loamy sand (Tables 3 and 4). P1 has fine roots in  
277 all horizons.

278 The profile P2 is better developed with a thicker B horizon. The cambic horizon exhibits weakly expressed  
279 stagnic properties, in which redoximorphic features (Fe mottling) make up a minor portion of the soil volume  
280 (Table 4). In contrast to P1, profile P2 predominantly has fine and medium roots.

281 Profile P3 is classified as Entic Podzol (Arenic). It presents a weakly-moderately developed 3Bs horizon that  
282 fulfils, at least partially, the requirements of a spodic horizon with the colour (7.5YR4/6), pH (5.0) and organic  
283 carbon content (12 g/kg). It has a transitional EB horizon that overlies the Bs horizon. P3 exhibits a high  
284 abundance of fine, medium and coarse roots that are concentrated in the A and 2EB horizons (Table 3).  
285 Similarly to the vegetation cover (Table 1), the abundance of roots in the soils (Table 3) increased from  
286 profile 1 to profile 3.

287

#### 288 4.3. $^{240}\text{Pu}/^{239}\text{Pu}$ ratio and $^{239+240}\text{Pu}$ inventories

289 The distribution of the  $^{240}\text{Pu}/^{239}\text{Pu}$  atomic ratios for all samples (reference and erosion sites) exhibits slight  
290 increases with depth: 0 – 5 cm =  $0.15 \pm 0.02$ ; 5 – 10 cm =  $0.17 \pm 0.02$ ; 10 – 15 cm =  $0.20 \pm 0.05$ ; 15 – 20 cm  
291 =  $0.19 \pm 0.04$ . In general, the  $^{239+240}\text{Pu}$  activities of all reference and erosion sites show the same distribution  
292 trend with depth: Pu activities are higher at the soil surface (0 – 5 cm) and decrease exponentially with depth  
293 (Fig. 2). Only the erosional site at Temple Lake shows a relatively high  $^{239+240}\text{Pu}$  activity at 10 – 15 cm, but  
294 having also a large error range.

295 Compared to the reference sites, the erosion sites of the Alice Lake and Temple Lake moraines exhibit lower  
296 total Pu inventories. This is not the case for the Lonesome Lake site, where the erosional and reference sites  
297 exhibit similar values (Fig. 2).

298

#### 299 4.4. Rates of soil erosion and accumulation

300 The  $^{239+240}\text{Pu}$  inventories on these moraines clearly indicate a considerable decrease in net soil erosion with  
301 increasing age, regardless of the model used (Fig. 3). The Pu inventories in fact indicate an overall mass  
302 loss or gain and, thus, a change in mass of a specific soil. The change in the Pu inventory or soil mass (M) is  
303 given by:

$$304 \frac{dM}{dt} = D(t) - E(t) - L(t) \quad (5)$$

305 with  $D(t)$  = dust input,  $E(t)$  = erosion rate,  $L(t)$  = leaching rate. Due to the insolubility of Pu, leaching rates can  
306 be assumed to be negligible.

307 Soils on the Alice Lake (P1) and Temple Lake (P2) moraines show negative values that indicate more soil  
308 erosion than accumulation. Both of these tundra sites show high mass losses and thus net erosion rates  
309 (values range from 517 to 257 t/km<sup>2</sup>/a and 172 to 72 t/km<sup>2</sup>/a). The forested site on the Lonesome Lake  
310 moraine exhibits values that are close to zero or slightly positive, indicating some minor soil accumulation  
311 (rates between 15 and 48 t/km<sup>2</sup>/a). Higher net rates (erosion, accumulation) were obtained for all sites when

312 using the IM with the particle size correction factor  $P = 1$ , when compared to factors of  $P = 1.2$  or  $P = 1.5$   
313 (Fig. 3). When we applied the PDM model to the  $^{239+240}\text{Pu}$  data, the mass redistribution rates generally  
314 followed the same trend with time. The erosion rate was higher for the Alice Lake profile (average of 517  
315  $\text{t}/\text{km}^2/\text{a}$ ) and lower for the Temple Lake profile (average of 72  $\text{t}/\text{km}^2/\text{a}$ ).

316

#### 317 4.5. Correlation between soil organic carbon and $\delta^{13}\text{C}$

318 The  $\delta^{13}\text{C}$  values for the reference sites on the Alice Lake and Temple Lake moraines generally increased  
319 with depth and ranged between -28 ‰ and -24 ‰. The  $\delta^{13}\text{C}$  values varied less in the profile on the  
320 Lonesome Lake moraine. The erosion site on the Alice Lake moraine showed a similar trend, but with less  
321 variation. The erosion site on the Temple Lake moraine shows an inversion of the 0-5 cm and 5-10 cm  
322 samples.  $\delta^{13}\text{C}$  values from soil horizons at the reference and erosional sites on the Lonesome Lake moraine  
323 are generally similar, but the erosional site shows more variability.

324 Surprisingly, the correlation between C% and  $\delta^{13}\text{C}$  becomes weaker at all reference and erosion sites on  
325 older moraines (Fig. 4). Overall, the tundra reference sites show negative correlations between OC and  $\delta^{13}\text{C}$ .  
326 Among all sites, the reference site on the Alice Lake moraine has the highest correlation ( $R^2 = 0.88$ ) while  
327 the correlation for the corresponding erosional site is only  $R^2 = 0.34$ . The Temple Lake moraine shows a  
328 moderately negative correlation at the reference site ( $R^2 = 0.51$ ) and a very weak positive correlation at the  
329 erosional site ( $R^2 = 0.13$ ). At Lonesome Lake, the most notable pattern is seen in the noticeably higher OC  
330 value of the 0-5 cm samples when compared to the subsurface (especially in the reference profile).

331

332

## 333 5. Discussion

### 334 5.1. Onset of soil formation

335 The  $^{10}\text{Be}$  surface exposure dating provided an updated chronology for the moraines in the Cirque of the  
336 Towers (WRR) and, therefore, the timing for the onset of soil formation. Our results indicate that some of  
337 these moraines are older than previously estimated (Dahms et al., 2010). The Alice Lake moraine now  
338 appears to correspond to the IACP-Younger Dryas cooling event and not to a Holocene 'Neoglacial' period  
339 as previously reported (Dahms et al., 2010). The Temple Lake and Lonesome Lake moraines now appear to  
340 be roughly coeval to the Oldest Dryas (Shakun and Carlson, 2010), although the period of glacier recession  
341 and re-advance between 15 and 18 ka may more properly be termed "pre- Bølling-Allerød" (Rasmussen et  
342 al., 2014). These are so far some of the very few numerical dating attempts of lateglacial moraines in the

343 Wind River Range. The Temple Lake and Lonesome Lake moraines, although separated over a relatively  
344 long distance (approximately 1 km), also represent several re-advance phases during the Oldest Dryas.  
345 However, the term 'Oldest Dryas' is poorly defined and should, according to Rasmussen et al. (2014), not be  
346 used. This episode was defined as a period of biostratigraphic change reflected in terrestrial records in  
347 Denmark (Iversen, 1954). The period between 15 and 18 ka belongs to a general period with glacier  
348 recession and re-advances.

349 The moraines we sampled in Cirque of the Towers correspond to the pre- Bølling–Allerød and IACP-  
350 Younger Dryas cooling phases and, at least in the investigated valley, deposits corresponding to a Holocene  
351 'Neoglacial' cold period are no longer identified (Dahms et al., 2018).

352

### 353 5.2. Provenance and distribution of Pu isotopes

354 Surface soils (0-5 cm), containing the majority of the  $^{239+240}\text{Pu}$  inventory, exhibited  $^{240}\text{Pu}/^{239}\text{Pu}$  ratios of  $(0.15$   
355  $\pm 0.02)$ , which appear to be slightly lower than the well-established global fallout range of  $0.18 \pm 0.014$  for  
356 Northern Hemisphere mid-latitude fallout (Kelley et al., 1999). The data indicate a mixing between global  
357 fallout and tropospheric fallout originating from the Nevada Test Site fallout. Previous work in the western US  
358 (Ketterer et al., 2004) has demonstrated the presence of similar mixing in locations Nevada, Arizona and  
359 Utah. In general, the distribution of  $^{239+240}\text{Pu}$  activities in our reference profiles is consistent with reported  
360 trends in the literature where higher activity is found at the soil surface exponentially decreasing with depth  
361 (Ketterer et al., 2004; Meusburger et al., 2016; Zollinger et al., 2015).

362 The total  $^{239+240}\text{Pu}$  inventories did not change along the investigated chronosequence and showed an  
363 average value close to  $200 \text{ Bq/m}^2$ . Plutonium is strongly retained in the upper 5 cm of the soils. Pu isotopes  
364 have a high ionic potential and strongly associate with specific soils phases such as iron/manganese oxides  
365 and humic substances (Ketterer et al., 2011). Because of the sizeable accumulation of organic matter in the  
366 A horizons, the potential translocation of Pu with percolating soil water appears to be strongly limited in these  
367 soils. As a consequence, a correlation between Pu and org. C was found (Fig. 4; all sites). Due to stronger  
368 disturbances at the erosional sites, this correlation was weaker. Furthermore, the  $^{239+240}\text{Pu}$  inventories that  
369 we measure in Cirque of the Towers are slightly higher than in other mountain regions in the Swiss Alps  
370 where about  $80\text{-}100 \text{ Bq/m}^2$  is often measured (Meusburger et al., 2016; Zollinger et al., 2015). The  
371 enhanced  $^{239+240}\text{Pu}$  inventories in the Wind River Basin are not unexpected, and could arise from the  
372 additional NTS input, as well as local/regional differences in local climate and precipitation patterns.

373

### 374 5.3. Evolution of soil erosion rates

375 The rates of soil erosion that we calculated for these soils declined noticeably with continued soil  
376 development over time and increased vegetation cover associated with natural successional changes. With  
377 the development of tundra and forest vegetation, soil erodibility apparently was drastically reduced.  
378 Vegetation and the observed changes in roots (density and thickness) certainly contributed to the decrease  
379 in erosion with increasing soil age. The measured rates of soil erosion for the younger soils (Cambisols) are  
380 comparable with Alpine soils that have developed in the active layer of permafrost (Zollinger et al., 2015). On  
381 the Alice Lake moraine, the erosion rates are in the range of 260 to 520 t km<sup>-2</sup> a<sup>-1</sup>. These are rather high  
382 values for natural and not human-affected alpine sites (Alewell et al., 2014; Zollinger et al., 2015). The  
383 observed changes in the vegetation type and cover (Table 1) certainly contributed to the decrease in erosion  
384 with increasing soil age.

385 The slightly positive values at the Lonesome Lake suggest both that the surface became stable and that the  
386 rates of dust accumulation outpaced erosion rates. Dust accumulation on soils have been reported in the  
387 WRR and its deposition is not only related to glacial episodes but is an ongoing process even in the post-  
388 glacial period (Applegarth and Dahms, 2004; Dahms and Rawlins, 1996). Dahms and Rawlins (1996)  
389 measured rates of modern dust deposition in the western slope of the WRR between 0.23 to 31.0 × 10<sup>-7</sup> g  
390 cm<sup>-2</sup> d<sup>-1</sup> for mineral dust which corresponds to 0.08 to 11.32 t km<sup>-2</sup> a<sup>-1</sup>. These rates have to be considered as  
391 minimum values, because the organic fraction was not included in their measurements. Brahney et al. (2015)  
392 inferred dust deposition rates for the last 2000 years of 0 – 4 t km<sup>-2</sup> a<sup>-1</sup> from lake sediments of two lakes in  
393 the Wind River Range. Apparently due to human impact, deposition rates at Lonesome Lake and North Lake  
394 increased to 25 and 58 t km<sup>-2</sup>, respectively, during the last few decades. Our measured soil accumulation  
395 rates at the Lonesome Lake site are in the range of 10 to 48 t km<sup>-2</sup> a<sup>-1</sup>. These values are close to the dust  
396 deposition rates determined by Dahms and Rawlins (1996) and Brahney et al. (2015). This furthermore  
397 suggests that the soils on the moraine slopes have little detectable erosion now, but receive some aeolian  
398 input that gives rise to a slightly positive mass balance. After more than 12 ka soil evolution, the moraine  
399 slopes have therefore become stabilised and may even exhibit a positive mass balance.

400 The δ<sup>13</sup>C-signature in topsoil layers showed values within the typical range of C<sub>3</sub>-plants (-20 to -30 ‰).  
401 Several studies have reported a close correlation between δ<sup>13</sup>C and soil organic matter at undisturbed sites,  
402 with an enrichment of <sup>13</sup>C with soil depth (Alewell and Schaub, 2009; Meusburger et al., 2013; Zollinger et  
403 al., 2015). In general, a better relationship between total soil organic carbon (SOC) and δ<sup>13</sup>C was obtained at  
404 the reference sites than at the erosional sites (Fig. 4). This indeed indicates that the distribution pattern of  
405 δ<sup>13</sup>C and total organic C was at least partially influenced by slope mass movement at the erosion sites. As

406 the relative proportion of  $^{13}\text{C}$  and  $^{12}\text{C}$  changes due to fractionation processes during the decomposition of  
407 SOC, SOC consequently becomes enriched in  $^{13}\text{C}$  relative to  $^{12}\text{C}$  as decomposer organisms preferentially  
408 utilise the lighter isotopic species, which has a lower dissociation energy and therefore requires less energy  
409 to be broken from their molecules (Alewell and Schaub, 2009). Furthermore, our results provide evidence  
410 that the relationship of SOC and  $\delta^{13}\text{C}$  weakens with soil age, i.e. from profile P1 to P3. This is a surprising  
411 result as we expected the contrary trend. We show that erosion rates distinctly decrease with soil age (Fig.  
412 3). Consequently, a better correlation between  $\delta^{13}\text{C}$  and organic C should be expected at both the reference  
413 and 'erosional' sites (Zollinger et al., 2015). The approach of SOC and  $\delta^{13}\text{C}$  gives, at its best, only qualitative  
414 indications about soil erosion. The unexpected trend seems to contradict the Pu-results. The erosion signal  
415 in  $\delta^{13}\text{C}$  however seems to be rather overshadowed by other processes with time. With increasing time and  
416 stabilisation of the slopes, the distribution of organic carbon and  $\delta^{13}\text{C}$  along the profile should approach a  
417 quasi-steady state situation that follows a clear depth pattern and thus close relation between org. C and  
418  $\delta^{13}\text{C}$  (Poage and Feng, 2004). This is, however, not the case and might be due either to increased  
419 bioturbation with increasing soil age or an increased accumulation of aeolian material with time that changes  
420 the relationship between SOC and  $\delta^{13}\text{C}$ . Over a longer-term, cryoturbation may also disturb the  $\delta^{13}\text{C}$   
421 distribution. Cryogenesis is often the controlling factor in patterned ground formation which also results in  
422 cryoturbated soil profiles, cryostructures and carbon sequestration (Ping et al. 2008). Plutonium integrates  
423 mass movements for the last about 5 decades whereas carbon isotopes cover a longer time period (up to  
424 century or even millennia). Therefore, carbon isotopes may also reflect other processes than only erosion  
425 (Alewell and Schaub, 2009; Alewell et al., 2014).

426

#### 427 5.4 Soil evolution since the late Pleistocene

428 In general, the soils showed greater profile differentiation and a higher degree of rubification and consistency  
429 (Table 3) with increasing age. These trends are consistent with results obtained in previous studies from the  
430 WRR (Dahms, 2002; Dahms et al., 2012). Furthermore, the soil evolutionary pathway — from Lithosols to  
431 Cambisols towards Podzols — found here is similar to those in European cold alpine environments (Dahms  
432 et al., 2012). Due to the higher levels of precipitation and lower rates of dust deposition, Podzols in the  
433 European Alps require much less time to develop than in the WRR (Dahms et al., 2012).  
434 Dahms (2002) and Dahms et al. (2010) studied soils elsewhere in the WRR and demonstrated that soils on  
435 Temple Lake moraines usually present a slightly higher degree of development (e.g. in terms of the silt and  
436 clay content) than Alice Lake moraine soils. Usually, argic horizons were reported for Temple Lake soils. The



437 profiles P1 and P2 did not present a typical Bt horizon. According to Birkeland (1984), aeolian input in  
438 gravelly parent materials (e.g. till) accelerates the formation of Bt horizons because the fine particles can  
439 easily infiltrate and accumulate downward in the soil profile. This process results in a well-known feature in  
440 some alpine soils of the Rocky Mountains, the so-called 'mixed loess' (Shroba and Birkeland, 1983).  
441 However, this feature could also be due to layering. In an allochthonistic approach, relatively sharp  
442 boundaries within soil profiles, marking abrupt changes in soil physical and chemical properties, frequently  
443 originate from discontinuities rather than exclusively from pedogenic processes (Lorz et al., 2013). Soils  
444 formed in cover-bed successions have layered parent materials with such discontinuities.

445 The presence of lithologic discontinuities in all soil profiles, evidenced by a change in the coarse fragment  
446 content and in the sand fractions, suggests that they have formed two different parent materials. The  
447 following processes may have been the cause for the formation of these lithologic discontinuities:

448 i) Aeolian input: due to the relatively dry conditions in the whole mountain range and surroundings,  
449 dust input is quite common here (Dahms and Rawlins, 1996). In addition, some local loess input  
450 during deglaciation also might have been possible. Although there is no distinct loess mantle  
451 covering the soils (because of aeolian fines being mixed into the till), it might be possible that the A  
452 and 2B horizons which exhibit a higher proportion of silt and clay content than their underlying  
453 horizons (Table 4) have been overprinted by dust input giving rise to stratification.

454 The soils may have lost part of their upper horizons by erosion episodes during periods of cold desiccating  
455 conditions (Younger Dryas or later stadials during the Holocene) with scarce deposition ( see also Hall,  
456 1999). A later period of deposition of a second material on top of the soil gives rise to an additional lithologic  
457 discontinuity. However, this remains slightly hypothetical because till often is layered. Hence, the substrate of  
458 P1, P2 and P3 was formed by a sequence of different processes that are typical for glacial and paraglacial  
459 environments. The glacial till was covered by sandy and silty sediments having a gravel content of < 10 %.  
460 This sandy-silty sediment has an aeolian origin and was partially mixed with the pre-existent till substrate,  
461 e.g., due to periglacially induced near-surfaces processes.

462 Erosion rates are very high at site P1. Nonetheless, the rate of pedogenesis was still sufficient to form a  
463 shallow Cambisol about 40 cm thick. Over time, the strong soil erosion caused less-weathered substrate to  
464 come closer to the land surface, so that soil is continuously rejuvenated. Due to the earlier stabilisation of the  
465 land surface by vegetation and roots at P3, soil erosion rates are now lower than accumulation rates (Fig. 3).  
466 This stabilisation could explain the difference to site P2, where a Cambisol developed instead of a Podzol.

467  
468

## 469 **6. Conclusions**

470 We provide in this study the first description and quantification of the temporal evolution of soil erosion and  
471 consequent stabilisation of moraines slopes in an alpine region. Our results support the hypothesis that soil  
472 erosion rates decrease over time as soils develop. Weakly to moderately developed soils (Cambisols) on  
473 younger moraines under tundra vegetation show evidence of high erosion rates ( $260$  to  $520 \text{ t km}^{-2} \text{ a}^{-1}$ )  
474 whereas the soils (Podzol) on the older moraines under forest vegetation exhibit erosion rates that are close  
475 to zero or even slightly positive - indicating some weak net accumulation. Moraine slopes in the study area,  
476 therefore, apparently reach geomorphic stability after more than 12 ka of soil formation. After this time, soil  
477 erosion rates reach nearly zero and soils even seem to receive a slight excess input due to dust  
478 accumulation. Furthermore, we provide an updated chronology for the glacial deposits in the Cirque of the  
479 Towers (WRR) that indicates that they have to be associated to the Lateglacial (post-LGM) period.  
480 The correlation between  $\delta^{13}\text{C}$  and SOC shows that bioturbation and/or dust input becomes more effective  
481 with time. This is possibly why the expected increase in correlation between  $\delta^{13}\text{C}$  and org. C was not  
482 detected. Erosion caused soil rejuvenation during the early stages of soil development; but with time, and  
483 after stabilisation of the slopes, aeolian input then comes to dominate soil formation and leads to the  
484 development of a positive mass balance.

485

## 486 **Acknowledgments**

487 This research was supported by the Swiss Government Excellence Scholarship (2016.0646/Brazil/OP) for  
488 Raquel de Castro Portes and by the Foundation for Research in Science and the Humanities at the  
489 University of Zurich (grant number STWF-17-025). We thank Sandro Egli for the assistance during the  
490 fieldwork and Diogo Noses Spinola for comments and proofreading of the manuscript. Sampling was  
491 performed in the Washakie District of Shoshone National Forest under Special Use Permit #2037-01.

492

## 493 **References**

- 494 Alewell, C., Meusburger, K., Juretzko, G., Mabit, L., Ketterer, M.E., 2014. Suitability of  $^{239+240}\text{Pu}$  and  $^{137}\text{Cs}$  as  
495 tracers for soil erosion assessment in mountain grasslands. *Chemosphere* 103, 274–280.  
496 doi:10.1016/j.chemosphere.2013.12.016
- 497 Alewell, C., Schaub, M., 2009. Stable carbon isotopes and oxygen isotopes as an indicator for soil  
498 degradation. *Rapid Commun. Mass Spectrom.* 24, 3567–3577. doi:10.1002/rcm
- 499 Applegarth, M.T., Dahms, D., 2004. Aeolian modification of moraine soils, Whiskey Basin, Wyoming, USA.

500 Earth Surf. Process. Landforms 29, 579–585. doi:10.1002/esp.1052

501 Balco, G., Stone, J.O., Liftonl, N.A., Dunai, T.J., 2008. A complete and easily accessible means of  
502 calculating surface exposure ages or erosion rates from  $^{10}\text{Be}$  and  $^{26}\text{Al}$  measurements. *Quaternary*  
503 *Geochronology* 3, 174-195.

504 Birkeland, P.W., 1984. *Soils and Geomorphology*. Oxford University Press, New York.

505 Bockheim, J.G., 1980. Solution and use of chronofunctions in studying soil development. *Geoderma* 24, 71-  
506 85.

507 Brahney, J., Ballantyne, A.P., Kocielek, P., Leavitt, P.R., Farmer, G.L., Neff, J.C., 2015. Ecological changes  
508 in two contrasting lakes associated with human activity and dust transport in western Wyoming.  
509 *Limnology and Oceanography* 60, 678-695.

510 Chmeleff, J., von Blanckenburg, F., Kossert, K., Jakob, D., 2010. Determination of the  $^{10}\text{Be}$  half-life by  
511 multicollector ICP-MS and liquid scintillation counting. *Nucl. Instrum. Methods Phys. Res. Sect. B* 268,  
512 192–199.

513 Christl, M., Vockenhuber, C., Kubik, P.W., Wacker, L., Lachner, J., Alfimov, V., Synal, H.-A., 2013. The ETH  
514 Zurich AMS facilities: Performance parameters and reference materials. *Nucl. Instruments Methods*  
515 *Phys. Res. Sect. B Beam Interact. with Mater. Atoms* 294, 29–38.

516 Dahms, D.E., 2002. Glacial stratigraphy of Stough Creek Basin, Wind River Range, Wyoming.  
517 *Geomorphology* 42, 59–83.

518 Dahms, D.E., Rawlins, C.L., 1996. A two-year record of eolian sedimentation in the Wind River Range,  
519 Wyoming, USA. *Arct. Alp. Res.* 210–216.

520 Dahms, D., Egli, M., Fabel, D., Harbor, J., Brandova, D., De Castro-Portes, R., Christl, M., (In Press) 2018.  
521 Revised Quaternary glacial succession and post-LGM recession, southern Wind River Range,  
522 Wyoming, USA. *Quaternary Science Reviews*.

523 Dahms, D., Favilli, F., Krebs, R., Egli, M., 2012. Soil weathering and accumulation rates of oxalate-  
524 extractable phases derived from alpine chronosequences of up to 1Ma in age. *Geomorphology* 151–  
525 152, 99–113. doi:10.1016/j.geomorph.2012.01.021

526 Dahms, D.E., Birkeland, P.W., Shroba, R.R., Miller, C.D., 2010. Latest Quaternary glacial and periglacial  
527 stratigraphy, Wind River Range, Wyoming, Wyoming: Geological Society of America Digital Map and  
528 Chart Series. doi:10.1130/2010.DMCH007.TXT.

529 FAO, 2006. *Guidelines for soil description*. 4<sup>th</sup> ed., Rome.

530 Gosse, J.C., Phillips, F.M., 2001. Terrestrial in situ cosmogenic nuclides: theory and application. *Quat. Sci.*  
531 *Rev.* 20, 1475–1560.

532 Hall, R.D., 1999. Effects of Climate Change on Soils in Glacial Deposits, Wind River Basin, Wyoming. *Quat.*  
533 *Res.* 51, 248–261. doi:10.1006/qres.1999.2032

534 He, Q., Walling, D.E., 1997. The distribution of fallout <sup>137</sup>Cs and <sup>210</sup>Pb in undisturbed and cultivated soils.  
535 *Appl. Radiat. Isot.* 48, 677–690.

536 He, Q., Walling, D.E., 1996. Interpreting Particle Size Effects in the Adsorption of <sup>137</sup>Cs and Unsupported  
537 <sup>210</sup>Pb by Mineral Soils and Sediments 30, 117–137.

538 Huggett, R.J., 1998. Soil chronosequences, soil development, and soil evolution: A critical review. *Catena*  
539 32, 155–172. doi:10.1016/S0341-8162(98)00053-8

540 IUSS Working Group WRB, 2014. World reference base for soil resources 2014, World Soil Resources  
541 Reports. Rome.

542 Iversen, J., 1954. The Late-glacial Flora of Denmark and its Relation to Climate and Soil. *Danmarks*  
543 *Geologiske Undersøgelser, Række II*, 80.

544 Keefer, W.R., 1970. Structural Geology of the Wind River Basin, Wyoming Structural Geology of the Wind  
545 River Basin , Wyoming.

546 Kelley, J.M., Bond, L.A., Beasley, T.M., 1999. Global distribution of Pu isotopes and <sup>237</sup>Np. *Sci. Total*  
547 *Environ.* 237-238, 483–500.

548 Ketterer, M.E., Hafer, K.M., Link, C.L., Kolwaite, D., Wilson, J., Mietelski, J.W., 2004. Resolving global  
549 versus local / regional Pu sources in the environment using sector ICP-MS environment using sector  
550 ICP-MS. *J. Anal. At. Spectrom.* 19, 241-245.

551 Ketterer, M.E., Zheng, J., Yamada, M., 2011. Applications of Transuranics as Tracers and Chronometers in  
552 the Environment, in: Baskaran, M. (Ed.), *Handbook of Environmental Isotope Geochemistry*. Springer,  
553 p. 944.

554 Kohl, C., Nishiizumi, K., 1992. Chemical isolation of quartz for measurement of in-situ -produced cosmogenic  
555 nuclides. *Geochim. Cosmochim. Acta* 56, 3583–3587. doi:10.1016/0016-7037(92)90401-4

556 Lal, R., Elliot, W., 1994. Erodibility and erosivity, in: Lal, R. (Ed.), *Soil Erosion Research Method. Soil Water*  
557 *Conserv. Soc.*, St. Lucie Press, Delray Beach, Florida, pp. 181–208.

558 Lal, R., Wasson, R., Tims, S.G., 2013. Applicability of <sup>239</sup>Pu as a tracer for soil erosion in the wet-dry tropics  
559 of northern. *Nucl. Inst. Methods Phys. Res. B* 294, 577–583. doi:10.1016/j.nimb.2012.07.041

560 Lorz, C., Frühauf, M., Mailänder, R., Phillips, J.D., Kleber, A., 2013. Influence of cover beds on soils. In:  
561 Kleber, A., Terhorst, B. (eds), *Mid-latitude slope deposits (cover beds). Developments in*  
562 *Sedimentology* 66, 95-125.

- 563 Masarik, L., Wieler, R., 2003. Production rates of cosmogenic nuclides in boulders. *Earth and Planetary*  
564 *Science Letters* 216, 201-208.
- 565 Meusburger, K., Mabit, L., Ketterer, M., Park, J.H., Sandor, T., Porto, P., Alewell, C., 2016. A multi-  
566 radionuclide approach to evaluate the suitability of  $^{239+240}\text{Pu}$  as soil erosion tracer. *Sci. Total Environ.*  
567 566–567, 1489–1499. doi:10.1016/j.scitotenv.2016.06.035
- 568 Meusburger, K., Mabit, L., Park, J.H., Sandor, T., Alewell, C., 2013. Combined use of stable isotopes and  
569 fallout radionuclides as soil erosion indicators in a forested mountain site, South Korea. *Biogeosciences*  
570 10, 5627–5638. doi:10.5194/bg-10-5627-2013
- 571 Muhs, D., 2013. The geologic record of dust in the Quaternary. *Aeolian Research* 9, 3-48.
- 572 Nishiizumi, K., Imamura, M., Caffee, M.W., Southon, J.R., Finkel, R.C., McAninch, J., 2007. Absolute  
573 calibration of  $^{10}\text{Be}$  AMS standards. *Nucl. Instruments Methods Phys. Res. Sect. B Beam Interact. with*  
574 *Mater. Atoms* 258, 403–413. doi:10.1016/j.nimb.2007.01.297
- 575 Pigati, J.S., Lifton, N.A., 2004. Geomagnetic effects on time-integrated cosmogenic nuclide production with  
576 emphasis on in situ  $^{14}\text{C}$  and  $^{10}\text{Be}$ . *Earth Planet. Sci. Lett.* 226, 193–205.
- 577 Ping, C.L., Michaelson, G.J., Kimble, J.M., Romanovsky, V.E., Shur, Y.L., Swanson, D.K., Walker, D.A.,  
578 2008. Cryogenesis and soil formation along a bioclimate gradient in Arctic North America. *J Geophys*  
579 *Res-Bioge* 113, G03S12.
- 580 Poage, M.A., Feng, X., 2004. A theoretical analysis of steady state  $\delta^{13}\text{C}$  profiles of soil organic matter. *Global*  
581 *Biogeochemical Cycles* 18, GB2016, doi:10.1029/2003GB002195
- 582 Quine, T.A., Walling, D.E., 1991. Rates of soil erosion on arable fields in Britain: quantitative data from  
583 caesium-137 measurements. *Soil Use Manag.* 7, 169–176.
- 584 Rasmussen, S.O., Bigler, M., Blockley, S.P., Blunier, T., Buchardt, S.L., Clausen, H.B., Cvijanovic, I., Dahl-  
585 Jensen, D., Johnsen, S.J., Fischer, H., Gkinis, V., Guillevic, M., Hoek, W.Z., Lowe, J.L., Pedro, J.B.,  
586 Popp, T., Seierstad, I.K., Steffensen, J.P., Svensson, A.M., Vallelonga, P., Vinther, B.M., Walker,  
587 M.J.C., Wheatley, J.J., Winstrup, M., 2014. A stratigraphic framework for abrupt climatic changes  
588 during the Last Glacial period based on three synchronized Greenland ice-core records: refining and  
589 extending the INTIMATE event stratigraphy. *Quaternary Science Reviews* 106, 14-28.
- 590 Schaetzl, R.J. 1998. Lithologic discontinuities in some soils on drumlins: Theory, detection, and application.  
591 *Soil Science* 16: 570-590.
- 592 Shakun, J.D., Carlson, A.E., 2010. A global perspective on Last Glacial Maximum to Holocene climate  
593 change. *Quat. Sci. Rev.* 29, 1801–1816.
- 594 Shroba, R.R., Birkeland, P.W., 1983. Trends in late-Quaternary soil development in the Rocky Mountains

595 and Sierra Nevada of the western United States, in: Porter, S.C. (Ed.), Late-Quaternary Environments  
596 of the United States. University of Minnesota Press, Minneapolis.

597 Stone, J.O., 2000. Air pressure and cosmogenic isotope production. *J. Geophys. Res. Solid Earth* 105,  
598 23753–23759.

599 von Blanckenburg, F., Belshaw, N.S., O’Nions, R.K., 1996. Separation of  $^9\text{Be}$  and cosmogenic  $^{10}\text{Be}$  from  
600 environmental materials and SIMS isotope dilution analysis. *Chem. Geol.* 129, 93–99.

601 Walling, D., He, Q., 1999. Improved models for estimating soil erosion rates from cesium-137  
602 measurements. *J. Env. Qual* 28, 611–622.

603 Walling, D., Quine, T., 1990. Calibration of caesium-137 measurements to provide quantitative erosion rate  
604 data. *L. Degrad Rehabil* 2, 161–175.

605 Whittaker, R.H. 1962. Classification of natural communities. *Botan. Rev.* 28, 1-239.

606 Wischmeier W.H., Smith D.D., 1960. A universal soil loss estimating equation to guide conservation farm  
607 planning. *Proceedings of the 7th International Congress of Soil Science* 1, 418-425.

608 Zhang, X., Higgitt, DL, Walling, D.E., 1990. A preliminary assessment of the potential for using caesium-137  
609 to estimate rates of soil erosion in the Loess Plateau of China. *Hydrol Sci J* 35, :43–252.

610 Zollinger, B., Alewell, C., Kneisel, C., Meusbürger, K., Brandová, D., Kubik, P., Schaller, M., Ketterer, M.,  
611 Egli, M., 2015. The effect of permafrost on time-split soil erosion using radionuclides ( $^{137}\text{Cs}$ ,  $^{239+240}\text{Pu}$ ,  
612 meteoric  $^{10}\text{Be}$ ) and stable isotopes ( $\delta^{13}\text{C}$ ) in the eastern Swiss Alps. *J. Soils Sediments* 15, 1400–1419.  
613 doi:10.1007/s11368-014-0881-9

## Figure captions

**Figure 1.** a) Location of the Wind River Range (pink square) within North America. b) Regional location map of the Wind River Range. The pink square represents the location of the Cirque of the Towers. c) Detailed location map of the Cirque of the Towers showing the sampling sites. P1 – P3: investigated pedons. Close nearby to these pedons are the reference and erosion sites for Pu and  $\delta^{13}\text{C}$  measurements (Table 1); CT1 – CT6: sampled boulders (for  $^{10}\text{Be}$  dating).

**Figure 2.** Average  $^{239+240}\text{Pu}$  activity ( $\pm$  standard error) with soil depth and total inventory of the reference and erosional sites along the investigated sequence.

**Figure 3.** (a) Soil redistribution rates of the moraine study sites as a function of surface age. Negative values indicate soil erosion and positive values soil accumulation. The rates were calculated using the  $^{239+240}\text{Pu}$  inventories, the Profile Distribution Model (PDM) (Walling and Quine, 1990; Zhang et al., 1990) and the Inventory Model (IM) (Lal et al., 2013). The following particle size correction factors were considered:  $P = 1$  and  $P = 1.2$  (according to Walling and He, 1999) and  $P = 1.5$  (according to Lal et al., 2013). (b) Calculated mass fluxes in and out of the soils using the inventory method ( $P = 1$  to 1.5) and estimated dust deposits (based on Dahms and Rawlins (1996) and Brahney et al. (2015)). See also equation 5.

**Figure 4.** (a) Comparison between soil organic carbon (SOC) content and  $\delta^{13}\text{C}$  of the soil samples at the reference and erosion/accumulation sites and as function of sampling depth. (b) Correlation of  $^{239+240}\text{Pu}$  with organic C at the reference and erosion/accumulation sites.

Figure 1 (low-resolution)  
[Click here to download high resolution image](#)

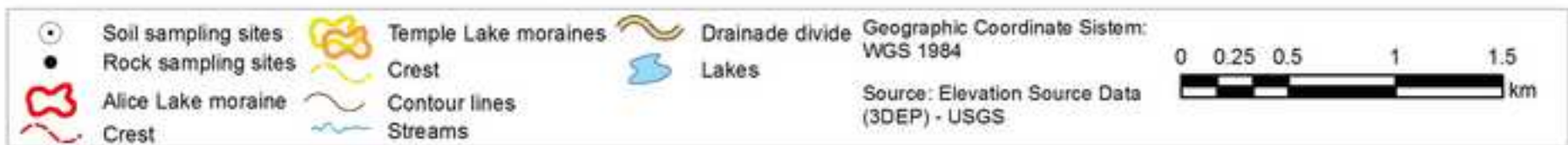
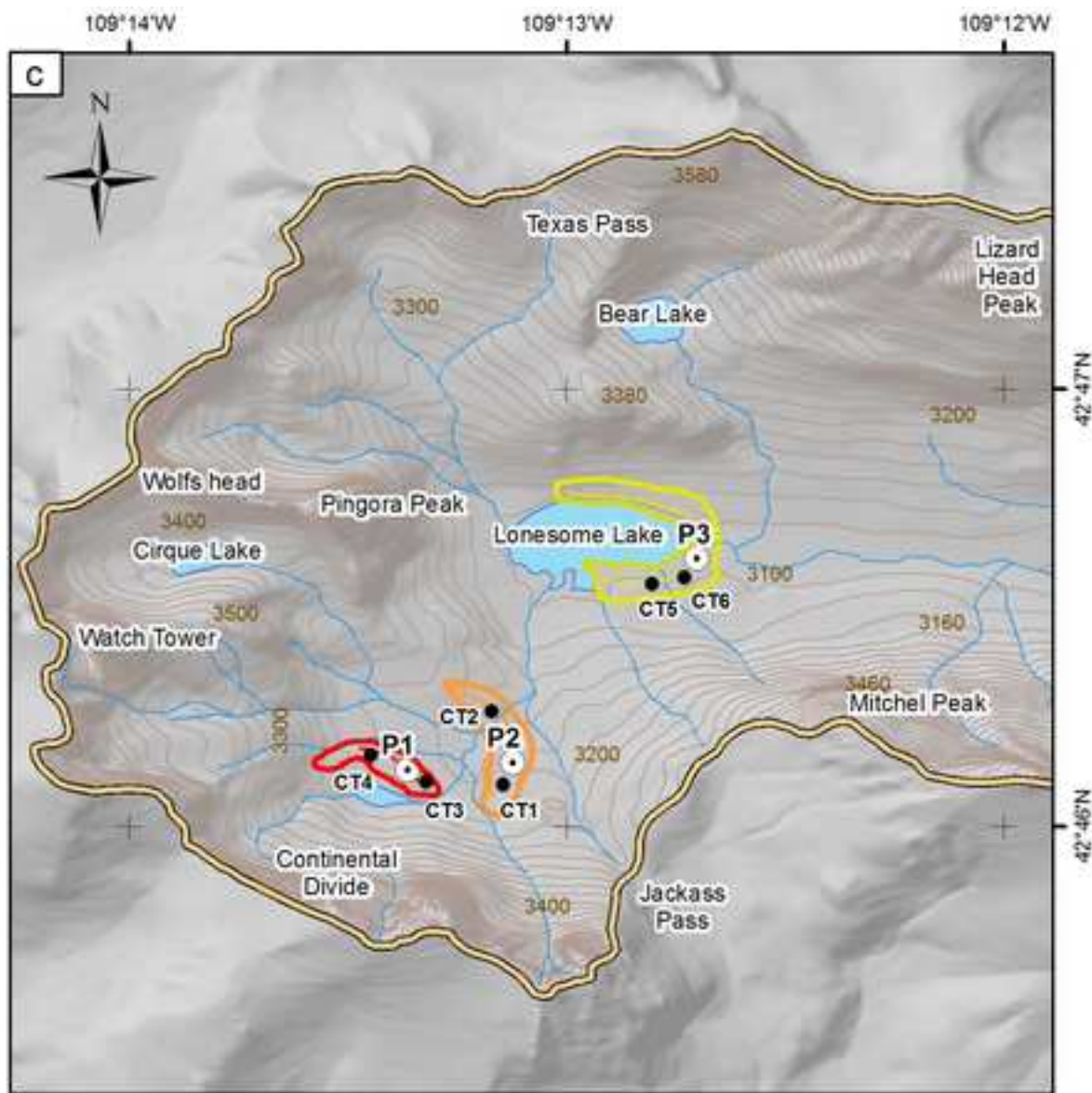
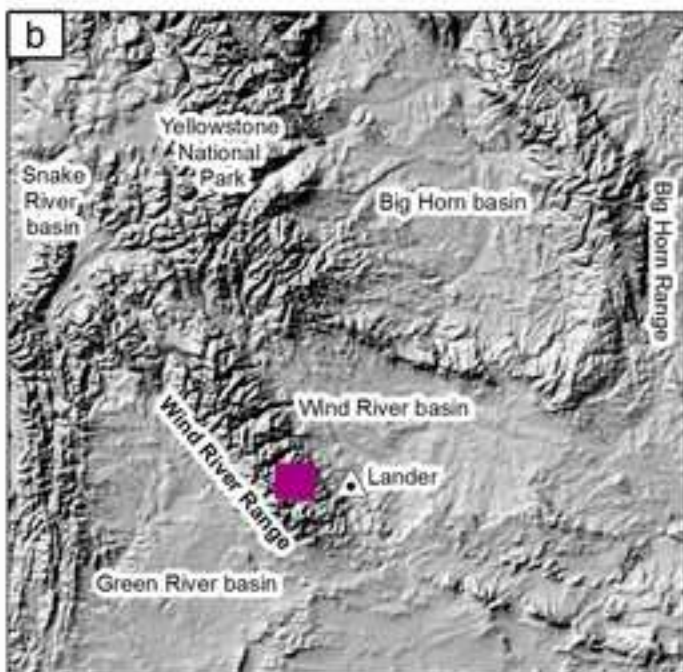




Figure 3 (low-resolution)

[Click here to download high resolution image](#)

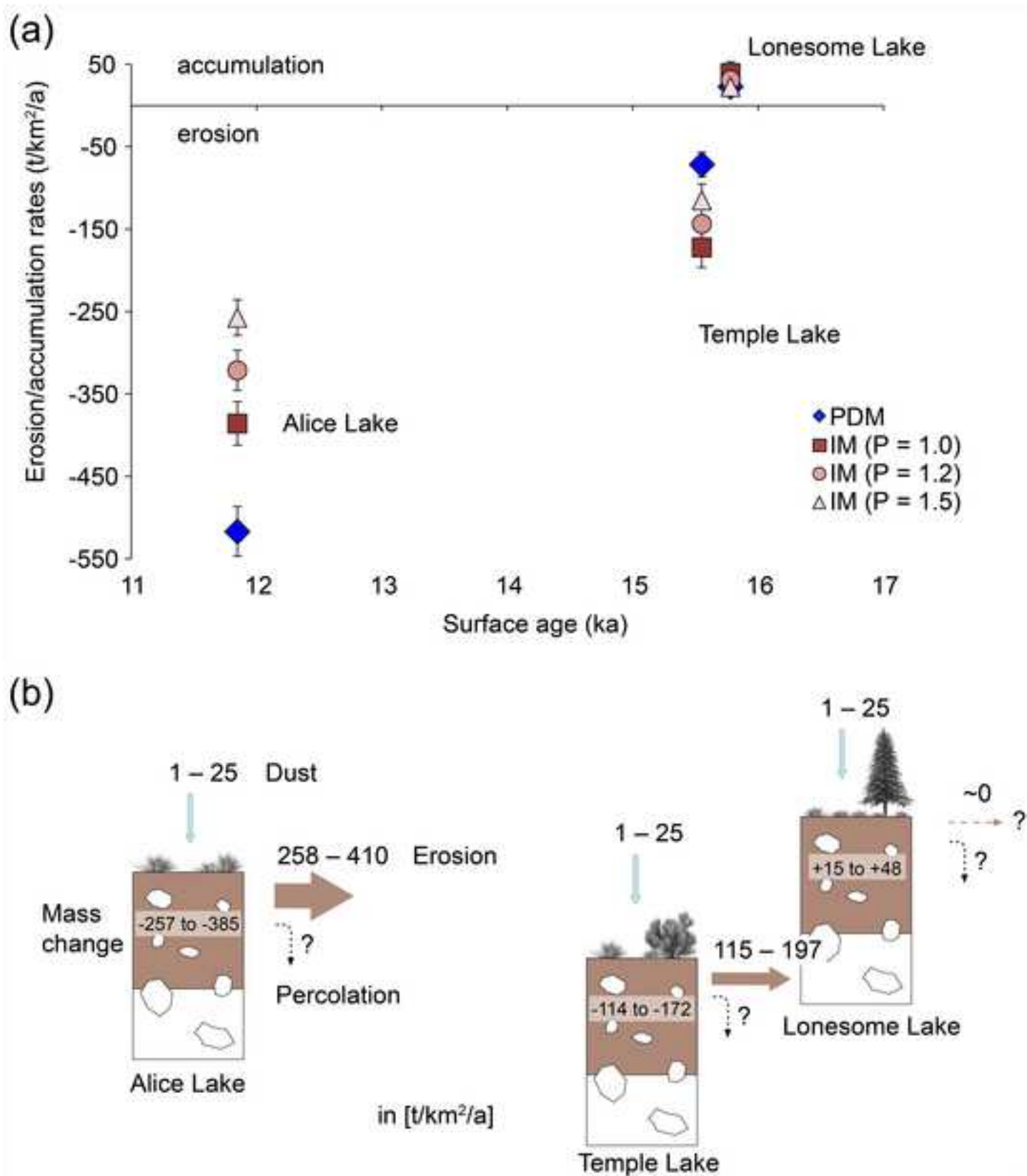


Figure 4 (low-resolution)

[Click here to download high resolution image](#)

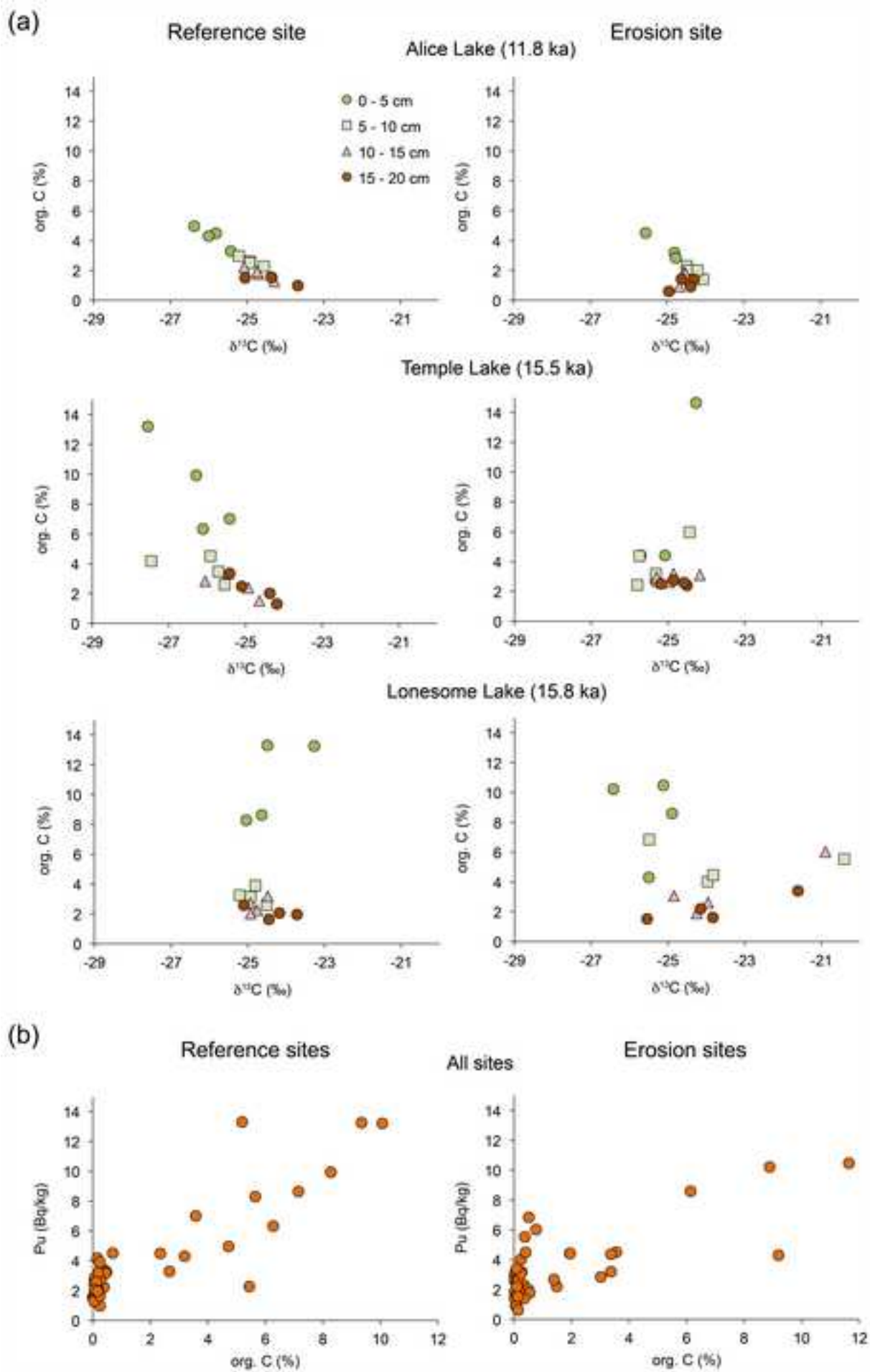
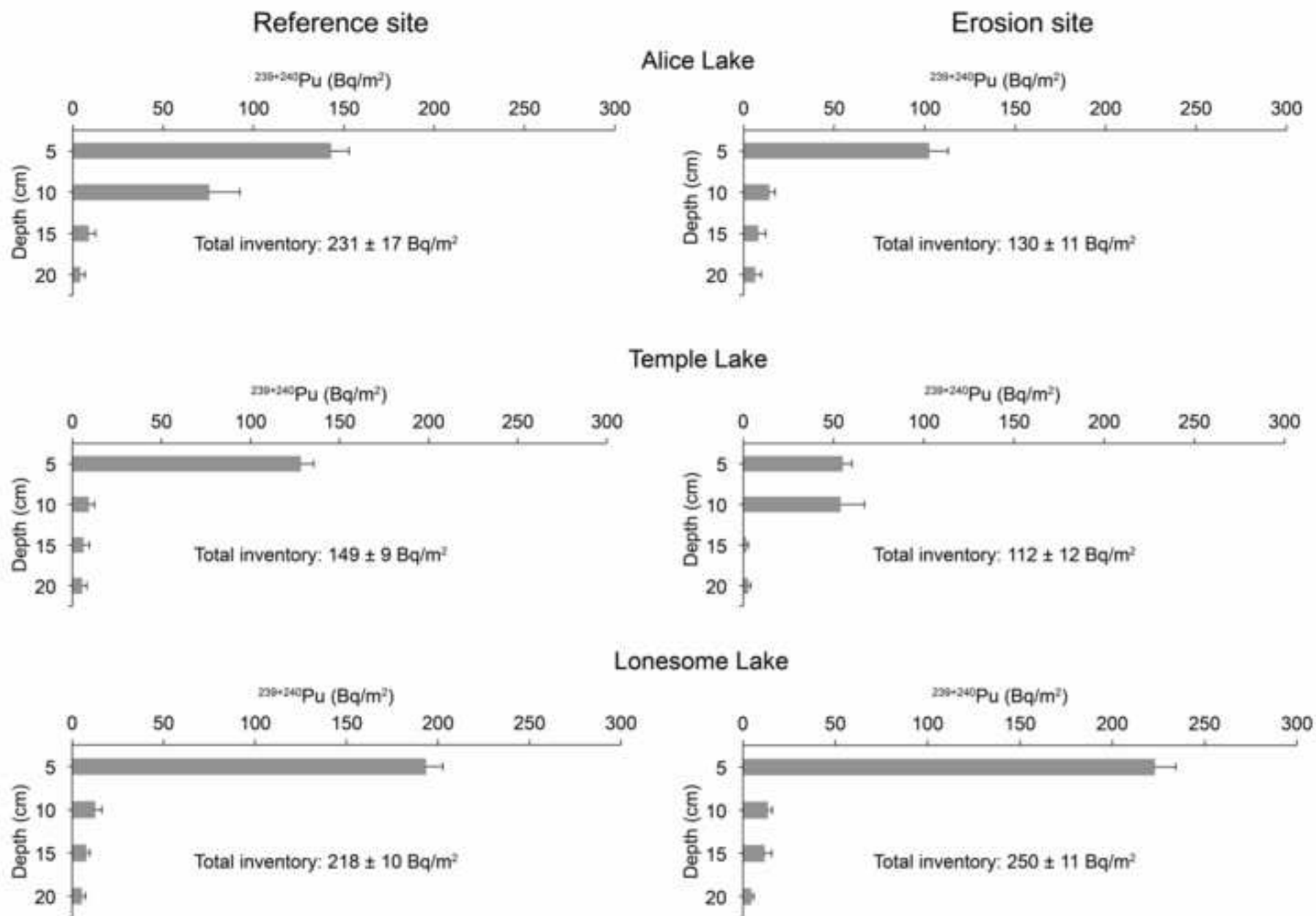


Figure 2 (low-resolution)  
[Click here to download high resolution image](#)



**Table 1.** Characteristics of the investigated sites of the Cirque of Tower, Wind River Range.

Site	Assumed age of the moraine (Dahms et al., 2010)	Pedon	Site type	Elevation (m a.s.l.)	Latitude/Longitude (°N/°E)	Landform	Aspect (°N)	Slope (%)	Slope position	Slope form	Slope length (m)	Parent material	Vegetation	Vegetation cover (%)
Alice Lake	Holocene	P1	Reference	3213	42.7687/-109.2229	End moraine	60	1	Crest	Flat	-	Granitic till	Alpine tundra	50
			Erosion	3210	42.7687/-109.2229	End moraine	60	25	Backslope	Straight	20	Granitic till	Alpine tundra	50
Temple Lake	Pleistocene	P2	Reference	3190	42.7683/-109.2182	Lateral moraine	350	3	Crest	Flat/ slightly concave	-	Granitic till	Alpine tundra/ Krummholz	72
			Erosion	3193	42.7683/-109.2182	Lateral moraine	350	27	Backslope	Straight	15	Granitic till	Alpine tundra/ Krummholz	72
Lonesome Lake	older than Temple lake	P3	Reference	3104	42.7770/-109.2130	End moraine	45	1	Crest	Flat	-	Granitic till	Montane forest	97
			Erosion	3100	42.7770/-109.2130	End moraine	45	27	Backslope	Straight	21	Granitic till	Montane forest	97

**Table 2**[Click here to download Table: Table\\_2.docx](#)**Table 2.**  $^{10}\text{Be}$  measurements of the moraine boulders of the Cirque of Towers, Wind River Range.

Site	Sample name	Latitude (°N)	Longitude (°W)	Elevation (m a.s.l.)	Sample thickness (cm)	Shielding correction	$^{10}\text{Be}^{\text{a, b}}$ ( $10^5$ atoms $\text{g}^{-1}$ qtz)	$^{10}\text{Be}$ surface exposure age <sup>c, d</sup> (a)
Alice Lake (P1)	CT3	42.76873	-109.2229	3225	1.8	0.930	$4.4 \pm 0.14$	$11285 \pm 1030$ (358)
Alice Lake (P1)	CT4	42.76873	-109.2229	3225	3.0	0.935	$4.8 \pm 0.19$	$12406 \pm 1174$ (499)
Temple Lake (P2)	CT1	42.76833	-109.2182	3216	2.5	0.947	$6.2 \pm 0.18$	$15937 \pm 1442$ (462)
Temple Lake (P2)	CT2	42.76828	-109.2176	3214	3.2	0.954	$5.9 \pm 0.20$	$15162 \pm 1395$ (507)
Lonesome Lake (P3)	CT5	42.72660	-109.2111	3125	3.0	0.972	$5.7 \pm 0.18$	$15253 \pm 1390$ (472)
Lonesome Lake (P3)	CT6	42.72660	-109.2111	3125	2.2	0.972	$6.1 \pm 0.19$	$16267 \pm 1483$ (504)

<sup>a</sup> We used a density of  $2.7 \text{ g cm}^{-3}$  for all samples.<sup>b</sup> Uncertainty includes AMS measurements errors and statistical counting error.<sup>c</sup> external (internal) uncertainty<sup>d</sup> We used zero rock erosion rates for all samples.<sup>e</sup> Surface exposure ages were calculated with the CRONUS-Earth online calculators (<http://hess.ess.washington.edu/>, Balco et al., 2008 and version 2.3) and using scaling scheme for spallation based on Lal (1991)/Stone (2000).

**Table 3**[Click here to download Table: Table\\_3.docx](#)**Table 3.** Soil physical, chemical and morphological properties of the investigated soils.

Pedon Horizon	Depth cm	Munsell color Moist	Bulk density g/cm <sup>3</sup>	Soil skeleton wt-% <sup>12</sup>	TOC <sup>1</sup> g/kg	pH <sup>2</sup>	Soil structure			Consistence		S <sup>8</sup>	P <sup>9</sup>	Roots	
							Grade <sup>3</sup>	Type <sup>4</sup>	Size <sup>5</sup>	Dry <sup>6</sup>	Moist <sup>7</sup>			A <sup>10</sup>	S <sup>11</sup>
P1 Alice Lake - Cambisol (Humic, Loamic)															
A1	0-15	10YR3/1	1.0	4.6	29.2	5	WE	SG	-	LO	VFR	NST	NPL	M	F
2A2	15-28	10YR3/2	1.1	12.2	14	5.4	WM	GR	FI	SO	VFR	NST	NPL	M	F
2Bw	28-43	10YR4/4	1.1	31.9	6.5	5.3	WM	GR	FI	SO	FI	SST	PL	M	F
3Cox/Bw	43-70+	10YR3/4	1.3	38.3	2.5	5.3	WE	GR	FI	SO	VFR	NST	NPL	C	F
P2 Temple Lake - Protostagnic Cambisol (Humic, Loamic, Raptic)															
A	0-17	10YR2/1	0.8	8.4	51.9	4.3	WE	GR	FI	LO	FR	NST	NPL	M	F, M
2Bwg1	17-40	10YR3/3	0.7	3.4	23.3	4.4	WM	GR	FI	SO	FI	SST	PL	M	F, M
3Bwg2	40-78+	10YR3/6	0.9	6.4	21.8	4.7	WE	GR	FI	SO	FR/FI	SST	SPL	M	F, M
P3 Lonesome Lake - Entic Podzol (Arenic)															
O	0-5	10YR2/2	-	6.5	110.4	4.5	WE	SG	-	LO	LO	NST	NPL	M	F, M, C
A	5-17	10YR3/3	0.8	6.5	29.3	4.7	WE	GR	FI	SO	FR	SST	NPL	M	F, M, C
2EB	17-30	10YR3/4	0.9	8.4	21.3	4.9	WE	GR	FI	SHA	FR	SST	NPL	M	F, M, C
3Bs	30-45	7.5YR4/6	1.2	17.6	12	5	WE	GR	FI	SHA	FR	SST	NPL	F	F, M, C
3Cox/B	45-55+	2.5Y4/4	1.7	20.1	3	5.8	WE	GR	FI	LO	LO	NST	NPL	F	F, M, C

<sup>1</sup>TOC = Total organic carbon.<sup>2</sup>pH CaCl<sub>2</sub>.<sup>3</sup>WE = Weak; WM = Weak to moderate.<sup>4</sup>SG = Single grain; GR = Granular.<sup>5</sup>FI = Fine/thin.<sup>6</sup>LO = Loose; SO = Soft; SHA = Slightly hard.<sup>7</sup>LO = Loose; VFR = Very friable; FR = Friable; FI = Firm.<sup>8</sup>S = Stickiness; NST = Non-sticky; SST = Slightly sticky.<sup>9</sup>P = Plasticity; NPL = Non-plastic; PL = Plastic.<sup>10</sup>A = Root abundance; F = Few; C = Common; M = Many.<sup>11</sup>S = Root size; F = Fine; M = medium; C = Coarse.<sup>12</sup>Material > 2 mm in diameter

**Table 4**  
[Click here to download Table: Table\\_4.docx](#)

**Table 4.** Particle-size distribution of the investigated soils.

Pedon/ Horizon	Depth	Particle-size distribution <sup>1</sup>											T <sup>2</sup>	CS/MS <sup>3</sup>	D <sup>4</sup>	CS/FS <sup>5</sup>	D <sup>6</sup>	MS/FS <sup>7</sup>	D <sup>8</sup>
		Sand	Very coarse sand	Coarse sand	Medium sand	Fine sand	Very fine sand	Silt	Coarse silt	Fine silt	Clay								
		g/kg	g/kg	g/kg	g/kg	g/kg	g/kg	g/kg	g/kg	g/kg	g/kg	g/kg							
P1 Alice Lake - Cambisol (Humic, Loamic)																			
A1	0-15	592	47	90	287	14	154	332	194	138	76	SL	0.3	17.8	6.4	183	20.3	243	
2A2	15-28	539	50	92	241	41	116	374	170	204	87	SL	0.4	9.3	2.3	15	5.9	6.3	
2Bw	28-43	515	57	92	219	35	112	380	164	216	105	L	0.4	5.4	2.6	35.6	6.3	38.9	
3Cox/Bw	43-70+	761	82	149	374	36	119	172	89	83	68	LS	0.4	-	4.1	-	10.3	-	
P2 Temple Lake - Protostagnic Cambisol (Humic, Loamic, Raptic)																			
A	0-17	529	66	96	202	86	79	335	109	226	136	SL	0.5	32.3	1.1	51	2.3	14.1	
2Bwg1	17-40	428	33	59	162	79	95	386	158	228	186	L	0.4	7.8	0.7	15.9	2.1	22	
3Bwg2	40-78+	590	59	90	268	102	71	354	137	217	56	SL	0.3	-	0.9	-	2.6	-	
P3 Lonesome Lake - Entic Podzol (Arenic)																			
O	0-5	-	-	-	-	-	-	-	-	-	-	-	-	-	-	-	-	-	
A	5-17	263	32	42	70	36	84	348	130	218	389	CL	0.6	17.2	1.2	29.1	2	14.4	
2EB	17-30	408	58	89	124	54	82	367	168	199	226	L	0.7	32	1.7	55.7	2.3	17.9	
3Bs	30-45	709	96	119	218	112	165	289	162	128	2	LS	0.5	16.2	1.1	11.8	2	5.3	
3Cox/B	45-55+	789	124	137	209	113	205	208	93	115	3	LS	0.7	-	1.2	-	1.9	-	

<sup>1</sup>Sand = 2000 - 63 µm; Very coarse sand = 2000 - 1250 µm; Coarse sand = 1250 - 630 µm; Medium sand = 630 - 200 µm; Fine sand = 200 - 125 µm; Very fine sand = 125 - 63 µm; Silt = 63 - 2 µm; Coarse silt = 63 - 20 µm; Fine silt = 20 - 2 µm; Clay = < 2 µm.

<sup>2</sup>T = Textural class; LS = Loamy sand; SL = Sandy loam; L = Loam; CL = Clay loam.

<sup>3</sup>Ratio of coarse sand to medium sand.

<sup>4</sup>Difference in the ratio of coarse sand to medium sand for the underlying and overlying horizon.

<sup>5</sup>Ratio of coarse sand to medium sand.

<sup>6</sup>Difference in the ratio of coarse sand to medium sand between the underlying and overlying horizon.

<sup>7</sup>Ratio of medium sand to fine sand.

<sup>8</sup>Difference in the ratio of coarse sand to medium sand between the underlying and overlying horizon.